Title

Erosion in southern Tibet shut down at ~10 Ma due to enhanced rock uplift within the Himalaya

Journal

Proceedings of the National Academy of Sciences of the United States of America, 112(39)

ISSN

0027-8424

Authors

Tremblay, Marissa M
Fox, Matthew
Schmidt, Jennifer L
et al.

Publication Date

2015-09-29

DOI

10.1073/pnas.1515652112

Peer reviewed

Erosion in southern Tibet shut down at ∼10 Ma due to enhanced rock uplift within the Himalaya

Marissa M. Tremblay[a,b,1], Matthew Fox[a,b], Jennifer L. Schmidt[c], Alka Tripathy-Lang[a,b], Matthew M. Wielicki[d], T. Mark Harrison[d,1], Peter K. Zeitler[c], and David L. Shuster[a,b]

[a]Department of Earth and Planetary Science, University of California, Berkeley, CA 94720; [b]Berkeley Geochronology Center, Berkeley, CA 94709; [c]Department of Earth and Environmental Sciences, Lehigh University, Bethlehem, PA 18015; and [d]Department of Earth, Planetary and Space Sciences, University of California, Los Angeles, CA 90095

Contributed by T. Mark Harrison, August 7, 2015 (sent for review June 19, 2015; reviewed by Bodo Bookhagen and Alison Duvall)

Exhumation of the southern Tibetan plateau margin reflects interplay between surface and lithospheric dynamics within the Himalaya–Tibet orogen. We report thermochronometric data from a 1.2-km elevation transect within granitoids of the eastern Lhasa terrane, southern Tibet, which indicate rapid exhumation exceeding 1 km/Ma from 17–16 to 12–11 Ma followed by very slow exhumation to the present. We hypothesize that these changes in exhumation occurred in response to changes in the loci and rate of rock uplift and the resulting southward shift of the main topographic and drainage divides from within the Lhasa terrane to their current positions within the Himalaya. At ∼17 Ma, steep erosive drainage networks would have flowed across the Himalaya and greater amounts of moisture would have advected into the Lhasa terrane to drive large-scale erosional exhumation. As convergence thickened and widened the Himalaya, the orographic barrier to precipitation in southern Tibet terrane would have strengthened. Previously documented midcrustal duplexing around 10 Ma generated a zone of high rock uplift within the Himalaya. We use numerical simulations as a conceptual tool to highlight how a zone of high rock uplift could have defeated transverse drainage networks, resulting in substantial drainage reorganization. When combined with a strengthening orographic barrier to precipitation, this drainage reorganization would have driven the sharp reduction in exhumation rate we observe in southern Tibet.

Tibet–Himalaya | thermochronometry | landscape evolution

The Himalaya–Tibet orogenic system, formed by collision between India and Asia beginning ca. 50 Ma, is the most salient topographic feature on Earth and is considered the archetype for understanding continental collision. Geophysical and geologic research has illuminated the modern structure and dynamics of the orogen (1). Nonetheless, how the relatively low relief and high elevation Tibetan plateau grew spatially and temporally and what underlying mechanism(s) drove the patterns of plateau growth remain outstanding questions.

In the internally drained central Tibetan plateau, evidence from carbonate stable isotopes suggest that high elevations persisted since at least 25–35 Ma (2, 3). Sustained high elevations since shortly after collision commenced have also been used to explain low long-term erosion rates in the internally drained plateau interior (4–6). In contrast to the central plateau, the externally drained Tibetan plateau margins serve as the headwaters for many major river systems in Asia. Because externally drained rivers provide an erosive mechanism to destroy uplifted terrane, understanding why these rivers have not incised further and more deeply into the Tibetan plateau is essential to decipher how the plateau grew. Recent research in the eastern (7, 8) and northern (9) Tibetan plateau indicates that erosion rates have increased significantly since ∼10 Ma. These increases suggest that rock uplift rates have also increased and that the plateau has expanded to the east and north during this time [due to lower crustal flow (7) or upper crustal extrusion (8) to the east and structural reorganization to the north (9)], causing rivers to steepen and erode at faster rates.

The history of the southern Tibetan plateau margin, on the other hand, is less well understood. The southern Tibetan plateau is presently drained by the Yarlung and Indus Rivers, which each flow parallel to the Himalayan range for more than 1,000 km before descending from the plateau at the Himalayan syntaxes. Evidence from fossils and carbonate stable isotopes suggest that high elevations in the southern Tibetan plateau persisted since at least 15 Ma (10, 11) and potentially even before collision began (12). Additionally, sediments from the Himalayan foreland, Bengal, and Central Myanmar basins require external drainage of the southern Tibetan plateau since at least 14 Ma and potentially as early as 40 Ma (13–15). High elevations and external drainage since at least Middle Miocene time indicate that rock uplift rates in the southern Tibetan plateau may have kept up with the pace of river incision for tens of millions of years. However, cosmogenic nuclide concentrations indicate low erosion rates (typically $<10^2$ m/Ma) in both the Indus and Yarlung drainages over the last several hundred thousand years (16, 17). No data yet exist to test whether these slow erosion rates persisted over longer 10^6- to 10^7-y timescales. Therefore, it is uncertain how high elevations in the southern plateau have been sustained: are long-term rock uplift and erosion rates both high or have slow erosion rates persisted despite external drainage by some other mechanism?

Here, we examine the exhumation history of the eastern part of the Tibetan plateau's southern margin using thermochronometry,

Significance

The Himalaya–Tibet plateau system formed by collision between India and Asia that began ca. 50 Ma and is still ongoing today. Despite being the most studied example of continent–continent collision, the evolution of topography in the Himalaya and Tibetan plateau remains an area of vigorous debate and active research. We present geochemical data on the cooling history of granites from the southern Tibetan plateau, which indicate that exhumation of these granites and therefore erosion rates in this region decreased significantly by ∼10 Ma after ∼5 Ma of rapid erosion. We hypothesize that this change in erosion rate reflects a tectonically imposed shift of the topographic and drainage divides south to their current positions within the Himalaya.

Author contributions: M.M.T., M.F., J.L.S., T.M.H., P.K.Z., and D.L.S. designed research; M.M.T., M.F., J.L.S., A.T.-L., M.M.W., T.M.H., P.K.Z., and D.L.S. performed research; M.M.T., M.F., J.L.S., A.T.-L., M.M.W., T.M.H., P.K.Z., and D.L.S. analyzed data; and M.M.T., M.F., J.L.S., A.T.-L., T.M.H., P.K.Z., and D.L.S. wrote the paper.

Reviewers: B.B., University of California, Santa Barbara; and A.D., Univ. Washington.

The authors declare no conflict of interest.

[1]To whom correspondence may be addressed. Email: mtremblay@berkeley.edu or tmark.harrison@gmail.com.

This article contains supporting information online at www.pnas.org/lookup/suppl/doi:10.1073/pnas.1515652112/-/DCSupplemental.

a technique in which thermal histories of rocks are constrained by the evolution of geochemical systems sensitive to temperatures within Earth's upper crust. We present apatite $^4He/^3He$, apatite and zircon (U-Th)/He, and biotite and K-feldspar $^{40}Ar/^{39}Ar$ thermochronometry data from granitic bedrock samples of the Cretaceous–Cenozoic Gangdese batholith in the eastern Lhasa terrane, southern Tibet. Samples were collected along a 1.2-km elevation transect near the eastern headwaters of the Lhasa River, a major tributary of the Yarlung River (Fig. 1 and *SI Appendix*, Table S1). This approach is advantageous for several reasons. First, by using a suite of thermochronometric systems sensitive to temperatures ranging from ~30 °C to 350 °C, we can identify changes in exhumation rate over a longer duration than would be possible with any subset of them. Second, sampling along an elevation transect leverages the fact that rocks at different elevations within a pluton share a similar exhumation history but have different cooling histories. Resolvable differences in the cooling histories between rocks at different elevations can more tightly constrain the overall exhumation history than the cooling history of a single elevation sample. Third, to avoid the effects of local-scale tectonic exhumation, we collected samples in a location that is not in the footwall of one of the north-south trending rift systems in southern Tibet. Therefore, the data primarily record temporal trends in erosional exhumation of the region. With data from this sampling scheme, we use 3D thermokinematic models to constrain the timing of both large-scale unroofing of the Gangdese batholith and local, kilometer-scale relief development due to river incision. From these data and thermokinematic models, we develop a hypothesis for landscape evolution within the southern Tibetan plateau that we illustrate schematically using a simple numerical model.

Thermochronometry

The thermochronometric data from the elevation transect and thermokinematic models are summarized in Figs. 2 and 3. Apatite (U-Th)/He and $^4He/^3He$ thermochronometry are sensitive to temperatures <100 °C and therefore reflect the thermal histories of rocks within the uppermost few kilometers beneath Earth's surface. Apatite (U-Th)/He ages from the sampling transect are relatively invariant with elevation, clustering between 16 and 11 Ma (Fig. 3*A* and *SI Appendix*, Table S5). Apatite $^4He/^3He$ thermochronometry provides information about both the (U-Th)/He age and radiogenic ^4He distribution of an apatite crystal (18); together these observations constrain the most recent cooling history of each sample between 80 °C and ~30 °C (for greater detail, see *SI Appendix*). Apatite $^4He/^3He$ data from five of the six transect samples (Fig. 2 and *SI Appendix*, Figure S1) are consistent with rapid cooling to near surface temperatures by 12–11 Ma (Fig. 2 *F–J*). $^4He/^3He$ release spectra of apatite crystals from the lowest elevation transect sample, MZ07, indicated significant zonation of the parent nuclides U and Th, which was confirmed by laser ablation U-Th mapping (*SI Appendix*, Fig. S2). The $^4He/^3He$ release spectra and U-Th maps for this sample are qualitatively consistent with rapid cooling to surface temperatures in the Middle Miocene as well.

The zircon (U-Th)/He and $^{40}Ar/^{39}Ar$ systems are sensitive to higher temperatures than the apatite (U-Th)/He system, providing information about rock thermal histories at deeper crustal levels. Unlike the apatite (U-Th)/He ages, which are relatively invariant with elevation and cluster in the Middle Miocene, zircon (U-Th)/He ages exhibit significant variation with elevation. The highest elevation sample MZ12 has a mean zircon (U-Th)/He age of 40.9 ± 3.5 Ma, whereas the lowest elevation sample MZ07 has a mean zircon (U-Th)/He age of 13.4 ± 1.9 Ma, which is indistinguishable from its apatite (U-Th)/He age (Fig. 3*A* and *SI Appendix*, Table S6). K-feldspar $^{40}Ar/^{39}Ar$ age spectra contain excess ^{40}Ar but portions are interpretable using the multidomain diffusion model (*SI Appendix*, Fig. S3) (19); overall the spectra are consistent with the pattern

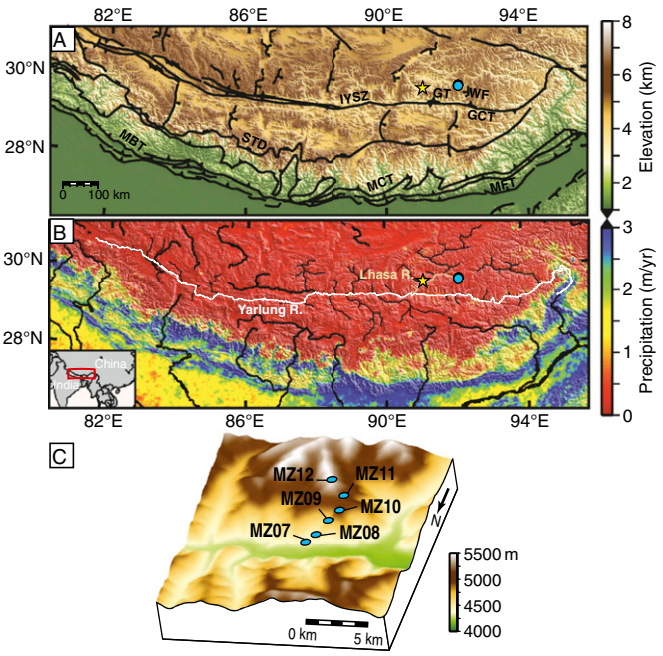

Fig. 1. (*A*) Topography and (*B*) mean annual precipitation (MAP) in southern Tibet and the Himalaya. The yellow star marks the city of Lhasa and blue circles denote the sample locations. The following generalized geologic structures are also shown in *A*: GCT, Great Counter Thrust; GT, Gangdese Thrust; IYSZ, Indus-Yarlung Suture Zone; MBT, Main Boundary Thrust; MCT, Main Central Thrust; MFT, Main Frontal Thrust; STD, South Tibetan Detachment; WF, Woka fault. In *B*, major river networks draining the southern Tibetan plateau and Himalaya are shown in black, with the Yarlung River and the Lhasa River highlighted in white and tan, respectively. *C* shows a detailed view of our sample locations and the surrounding topography. Topography plotted from 90 m SRTM (Shuttle Radar Topography Mission) data; MAP plotted from TRMM (Tropical Rainfall Measurement Mission) 2B31 data collected between 1998 and 2009 (36); geologic structures based on Styron et al. (30), Decelles et al. (31), Yin et al. (33), and Hodges (44).

seen in the zircon (U-Th)/He ages, with an older age spectrum characterized by less ^{40}Ar diffusion at the highest elevations and younger age spectra characterized by more ^{40}Ar diffusion at lower elevations. Biotite $^{40}Ar/^{39}Ar$ ages from three transect samples do not exhibit significant variation with elevation, with an average ages across samples of 60.5 ± 0.3 Ma (Fig. 3*A* and *SI Appendix*, Tables S7 and S8).

The differences in age–elevation relationships for this suite of thermochronometers document the complete cooling history of their host pluton and record major changes in cooling rate since collision between India and Asia commenced. The dataset requires at least three transitions in cooling rate. Pluton emplacement at 67.7 ± 2.5 Ma occurred at a depth of 12.5 ± 1.7 km, as determined by secondary ion mass spectrometry (SIMS) zircon U-Pb geochronology and Al-in-hornblende geobarometry respectively (*SI Appendix*, Table S2). The emplacement time and depth are consistent with initially rapid followed by declining postemplacement cooling recorded by all of the biotite ages and the K-feldspar $^{40}Ar/^{39}Ar$ data from the highest-elevation sample, which shows little evidence of diffusive ^{40}Ar loss. The K-feldspar $^{40}Ar/^{39}Ar$ spectra from lower-elevation samples (*SI Appendix*, Fig. S3) and the zircon (U-Th)/He ages document a period of slow cooling through the Paleogene. This slow cooling was followed by a sharp increase in cooling rate in the Neogene, as evidenced by the increase in age–elevation slope between the apatite and zircon (U-Th)/He systems (Fig. 3*A*). Finally, a sharp decrease in cooling rate of at least two orders of magnitude

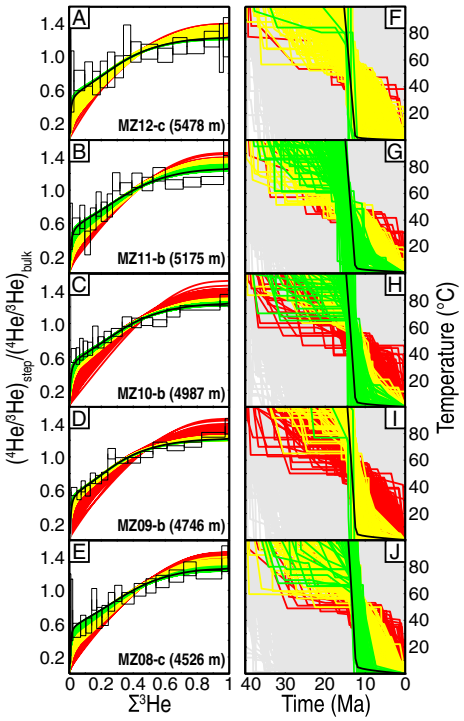

Fig. 2. Apatite $^4He/^3He$ thermochronometry of elevation transect samples. *A–E* show normalized $^4He/^3He$ ratios as a function of cumulative ^3He released during stepwise degassing analysis of each sample. *F–J* show 2,000 randomly generated cooling paths and their level of agreement with the observed $^4He/^3He$ data. Colored cooling paths predict the observed (U-Th)/He age within analytical uncertainty (1σ), whereas the gray paths do not. Green cooling paths are most consistent with the observed $^4He/^3He$ release spectra in the *Left Panels*; yellow and red cooling paths are progressively less consistent (for details, see *SI Appendix*). Black $^4He/^3He$ release spectra and cooling paths correspond to cooling paths shown in Fig. 3 that successfully predict the entire dataset. $^4He/^3He$ data from MZ07, the lowest elevation sample, indicate significant parent nuclide zonation; these data are shown in *SI Appendix*, Fig. S2 and are discussed in greater detail in *SI Appendix*.

by ∼10 Ma is documented by the thermal histories most consistent with the $^4He/^3He$ data (Fig. 2 *F–J*), with very little cooling occurring since this time.

Thermokinematic Histories and Their Regional Significance

We constructed 3D thermokinematic models using the finite-element code Pecube (20) to identify exhumation histories consistent with the observed suite of thermochronometric data (for details of modeling procedures, see *SI Appendix*). These models predict thermochronometric ages and account for both the effects of topography on the thermal structure of the crust and nonsteady geothermal gradients due to exhumation-driven heat advection. By confining the model domain to a 15 × 15-km region around the sample transect, we minimize uncertainties and complexities in boundary conditions associated with structures over longer lengthscales. Fig. 3 shows predicted ages (*A*) and the corresponding cooling paths (*B*) for geologic scenarios that successfully predict the entire dataset, minimizing the misfit between observed and predicted thermochronometric ages. We also consider geologic scenarios involving constant exhumation rates, and scenarios that are consistent with thermochronometric data from nearby regions including the internally drained portion of the Lhasa terrane (6), the eastern Himalayan syntaxis (21), and the eastern Tibetan plateau (22); we find that these latter scenarios are excluded by our dataset for this portion of the eastern Lhasa terrane (*SI Appendix*, Figs. S4 and S5).

Thermal paths that minimize the misfit between observed and predicted ages for this suite of thermochronometers involve cooling/exhumation between 0.2 and 0.5 km/Ma in the Late Cretaceous–Paleocene until 50–45 Ma, very slow exhumation (<0.01 km/Ma) from 50–45 to ∼17–16 Ma, rapid exhumation in excess of 1.0 km/Ma beginning at 17–16 Ma, and then very slow exhumation (<0.01 km/Ma and <750 m total) from 12–11 Ma to the present (*SI Appendix*, Figs. S5–S8). These conclusions are insensitive to the initial geothermal gradient (*SI Appendix*). We note that a portion of the cooling before 50–45 Ma, which we model as surface denudation in Pecube, must instead be associated with cooling of the batholith after emplacement at 12.5 ± 1.7-km depth at 67.7 ± 2.5 Ma. We are unable to resolve whether local relief was at steady state, increased during rapid exhumation between 17–16 and 12–11 Ma, or decreased during slow exhumation since 12–11 Ma. Importantly, the thermal histories most consistent with the $^4He/^3He$ data exclude significant recent relief development (Fig. 2 *F–J*), suggesting that the majority of the 1–2 km of relief in the eastern Lhasa terrane has persisted for ∼10 Ma.

Our thermochronometric data and modeling require two major changes in exhumation rate since the onset of India–Asia collision: a significant increase in exhumation rate at 17–16 Ma sustained for ∼5 Ma, followed by a significant slowing of exhumation since then. As our samples are in the hanging wall of the nearest major normal fault (Woka fault; Fig. 1*A*), we cannot explain these large-magnitude changes in exhumation rate simply as changes in local tectonic exhumation. Further, published thermochronometric data throughout the externally drained portion of the eastern (5, 23, 24) and central (25) Lhasa terrane, as well as the northeastern Tethyan Himalaya (26, 27), demonstrate that rapid exhumation rates (>1 km/Ma) were pervasive across the present day southern plateau between ∼20 and 10 Ma (see *SI Appendix*, Fig. S9 for sample locations). Notably, these exhumation rates are comparable to the more recent and currently active exhumation observed south of the present day topographic divide of the Himalaya (28). Our apatite $^4He/^3He$ data indicate that remarkably little exhumation has occurred in the

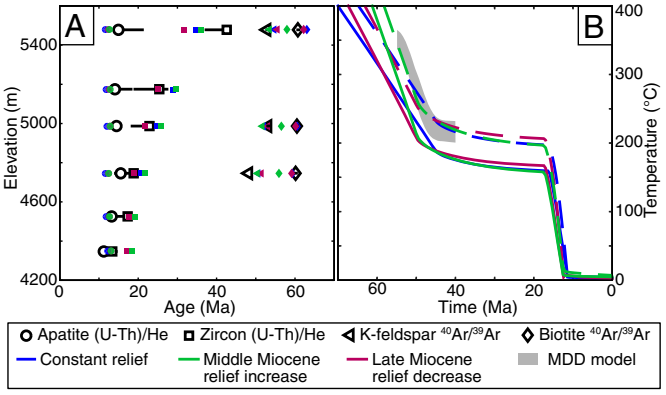

Fig. 3. (*A*) Observed (white) and modeled (color) apatite (U-Th)/He, zircon (U-Th)/He, K-feldspar $^{40}Ar/^{39}Ar$, and biotite $^{40}Ar/^{39}Ar$ ages as a function of elevation. We plot the median and range of observed individual crystal ages and the modeled ages for each sample. Model ages in *A* correspond to cooling paths in *B* generated using the 3D thermo-kinematic finite element modeling code Pecube (20). Geologic scenarios most consistent with the dataset are shown; other geologic scenarios are shown in *SI Appendix*, Fig. S4. Blue cooling paths are calculated for constant local relief; green paths include relief increase between 17–16 and 12–11 Ma; maroon paths include relief decrease since 11–12 Ma. We show cooling paths for the highest (MZ12, solid lines) and lowest (MZ07, dashed lines) elevation samples; cooling paths for all other samples would plot in between. The range of thermal paths modeled using a multiple diffusion domain (MDD) model for K-feldspars from MZ09 and MZ10 (*SI Appendix*, Fig. S3) is shown as a gray area in *B*.

southern Tibetan plateau since ca. 10 Ma, with the exception of localized tectonic exhumation within north-south trending normal fault systems (29, 30). Although an overall slowdown in exhumation was expected from previously published data (23, 25), the rapidity, magnitude, and duration of the decrease by 10 Ma required by our $^4He/^3He$ data have never before been documented and are not explicitly anticipated by existing models for the tectonic evolution of the southern Himalaya–Tibet orogen. The shutdown of erosion in southern Tibet since ∼10 Ma contrasts markedly with the exhumation histories in eastern and northern Tibet where significant increases in erosion rate since 10 Ma are documented (7–9), suggesting that disparate mechanisms drove exhumation across different regions of the Tibetan plateau.

A Landscape Evolution Hypothesis for Southern Tibet

We hypothesize that these two substantial changes in exhumation rate are a consequence of changes in rock uplift within the Himalaya and southern Tibet. Specifically, we suggest that the timing and distribution of rock uplift caused changes in both drainage network organization and orographic precipitation at the southern margin of the orogen, such that the main topographic and drainage divides shifted from within the Lhasa terrane to their present southerly positions within the Himalaya by 10 Ma. Below we describe details of this hypothesis and evidence that supports it.

Given that exhumation is the difference between rock uplift and surface uplift, two previously proposed scenarios for the tectonic evolution of southern Tibet can be called on to explain the rapid exhumation rates between 17–16 and 12–11 Ma that we observe. Carbonate stable isotopes suggest that elevations of the southern Tibetan plateau at this time were similar to modern elevations (10, 11); this implies that rock uplift and exhumation were roughly balanced, and therefore that rock uplift rates also exceeded 1 km/Ma across the southern Tibetan plateau between 17–16 and 12–11 Ma. Simultaneous rapid rock uplift and exhumation may have been caused by renewed underthrusting of Greater Indian lithosphere following a slab break-off event thought to have occurred during the Early Miocene (25, 31). However, initiation of rapid exhumation could also have lagged behind increased rock uplift rates, in which case surface elevations of the southern Tibetan plateau may have been significantly higher at the onset of rapid exhumation. The latter scenario is supported if rock uplift was associated with motion on the north-dipping Gangdese Thrust system (23, 32) (Fig. 1*A*), which is thought to have ceased by ∼23–18 Ma (32, 33). We cannot distinguish between these two mechanisms for rock uplift (renewed underthrusting and motion on the Gangdese thrust) on the basis of our data alone, but suggest that both could have contributed to the rock uplift that enabled the rapid exhumation recorded by our samples.

Regardless of the mechanism and timing of rapid rock uplift driving rapid exhumation between ∼17 and ∼11 Ma, it is important to recognize that erosion rates must have been fast at the time of rapid exhumation. Several aspects of the modern orogenic configuration—with the main topographic and drainage divides located within the Himalaya—would be prohibitive to such widespread rapid erosion. Although the Yarlung River drains $>10^5$ km^2 of the southern Tibetan plateau, its erosive capability upstream of the Namche Barwa massif is low (34), both because the Yarlung River currently has a relatively gentle channel slope (typically ∼0.1%) and because mean annual precipitation rates are <0.5 m/y and in many places <0.2 m/y across the drainage network (Fig. 1*B*) (35, 36). This precipitation regime is strongly controlled by orographic precipitation across the southern side of the Himalaya (35, 37). Although the southern Tibetan plateau may have received more precipitation in the past due to millennial scale climate variability (38), overall arid conditions have likely persisted on million-year timescales in the lee of the Himalaya orographic barrier. And although a general relationship between precipitation and erosion rates has not been identified, a global compilation of cosmogenic nuclide-derived erosion rates indicates that nowhere on Earth today do measured erosion rates equal or exceed 1.0 km/Ma where precipitation rates are <0.5 m/y (39).

A northward position of the main topographic and drainage divides, on the other hand, would enable high erosion rates across the southern Tibetan plateau before ∼10 Ma. Rather than being routed hundreds of kilometers to the east through the eastern Himalayan syntaxis, drainage networks originating in the southern Lhasa terrane could have followed more direct, southerly paths across the Himalaya. These proposed transverse rivers would necessarily have steeper longitudinal profiles, perhaps comparable to modern rivers draining the high Himalaya, and thus much higher erosive capability than the current configuration draining into the Yarlung River (34). Transverse rivers would also be effective at steering precipitation farther northward toward the interior of the plateau, analogous to transport of moisture up the Siang River valley within the eastern syntaxis today (Fig. 1*B*) (35). Additionally, a northward-shifted topographic divide may have resulted in a wetter precipitation regime in the southern Tibetan plateau, especially if there was a more gradual increase in elevation on the southern, windward side of the Himalaya at that time (37).

Although not explicitly considered in geologic studies of the Himalaya and sedimentary basins to the south, the pre-10-Ma drainage and topographic configuration we propose is consistent with observations from these regions. Steep transverse drainages originating within the Lhasa terrane would not only promote rapid erosion in southern Tibet but would also enable the well-documented rapid exhumation of the Greater Himalaya Sequence in the Middle Miocene, which experienced coeval rapid rock uplift due to motion on the Main Central Thrust (MCT; Fig. 1*A*) (40–43). Such a surface configuration would not necessarily imply low relief or low elevations across the Himalaya sequences before ∼10 Ma, because thrust faulting, crustal thickening, and exhumation within the Himalaya are well documented before and during this time (44, 45). Rather it suggests that the highest topography was located to the north within the Lhasa terrane, not unlike the modern orogen in which the highest deformation and exhumation rates are located south of the highest topography (28). Such a configuration would also have delivered material derived from the Lhasa terrane to the Himalayan foreland basin before ∼10 Ma, which sedimentary provenance studies document (13, 46). This configuration does not preclude the existence of a paleo-Yarlung River draining from the Lhasa terrane to the Bengal or Central Myanmar basins through the eastern Himalayan syntaxis (14, 15), but suggests that this river did not extend hundreds of kilometers to the west into the plateau interior.

The abrupt transition to extremely low exhumation rates ca. 10 Ma, and the persistence of low erosion rates since (Figs. 2 and 3), cannot be explained solely by changes in rock uplift within the southern Tibetan plateau, as erosion rates take time to respond to changes in rock uplift rate. For example, a regional-scale transition from north-south shortening to east-west extension across southern Tibet around 10 Ma (30) was most likely accompanied by decrease in rock uplift; however, we would expect erosion rates to remain high despite these low rock uplift rates as rivers incised deeper and further headward into the high-elevation plateau interior. We hypothesize that this transition was instead forced by substantial rock uplift in the Himalaya related to midcrustal duplexing in the Lesser Himalaya Sequence (41, 47). Rock uplift due to duplexing fast enough to outpace the incision of transverse drainage networks would result in large-scale drainage reorganization across the southern Tibetan plateau. Preexisting topography along the Indus–Yarlung Suture Zone

(IYSZ; Fig. 1*A*), associated with north-south extension in the latest Oligocene (31), may have been exploited during this drainage reorganization, routing rivers eastward and forcing them to combine with the Yarlung River and flow through the narrow eastern Himalayan syntaxis. Numerous geomorphic features, including the presence of barbed tributaries (*SI Appendix*, Fig. S10*E*), high elevation lakes (*SI Appendix*, Fig. S10*F*), and indicators of decreased carrying capacity, such as hillslopes that are steep but whose toes are buried beneath their own debris (*SI Appendix*, Fig. S10*G*) and anabranching, sediment choked rivers (*SI Appendix*, Fig. S10 *B* and *E*) suggest redirection of flow of major rivers draining the southern Tibetan plateau. Importantly, all of these features have been preserved due to slow erosion rates on the plateau since ∼10 Ma.

Two aspects of this proposed drainage reorganization would cause the observed shutdown of erosion in southern Tibet circa 10 Ma. First, the drainage network upstream of the eastern Himalayan syntaxis would significantly increase in length while draining a region at roughly the same elevations as before reorganization. As a result, channel slope and therefore stream power would transiently decrease in this upstream region. Simultaneously, this reorganization would have increased the drainage area upstream of the eastern Himalayan syntaxis; the resulting increase in stream power may have promoted the pulse of rapid exhumation from ∼10 to 6 Ma in the easternmost Himalaya (21) and enhanced the coupling between rapid rock uplift and erosion at the Namche Barwa massif (48). Second, precipitation would no longer be focused up transverse river valleys into the plateau interior. Because the orographic barrier to precipitation in southern Tibet strengthened as deformation to the south thickened and widened the Himalaya through the Middle Miocene, the steep drainages we envision would have provided the only channels for substantial moisture penetration to the north. Therefore, defeat of such transverse rivers would have cemented the orographic barrier and led to sustained aridification of the southern Tibetan plateau.

Rather than being transient, the low fluvial erosion rates that persist in the eastern Lhasa terrane have likely been sustained by the presence of a stationary, steepened reach or knickzone on the Yarlung River in the eastern Himalayan syntaxis. This knickzone results from coupling between focused rock uplift and rapid erosion within the syntaxis, creating a high-elevation base level for the drainage network upstream (49). On the basis of sediment fill immediately upstream of the knickzone, Wang et al. (50) call on knickzone generation at ∼2.5 Ma. However, we consider this as a minimum age because our thermochronometric data from much further upstream, as well as those of Zeitler et al. (21), suggest a sustained high-elevation base level for the Yarlung River in the eastern syntaxis since ∼10 Ma. Persistence of this stationary knickzone also prevents precipitation within the Yarlung River valley from being transported further upstream (Fig. 1*B*), maintaining arid conditions and low erosion rates in the plateau interior.

To illustrate how our postulated spatial and temporal changes in rock uplift rate would affect drainage networks, we performed numerical landscape evolution simulations with the model DAC (divide and capture) (51). These simulations are not designed to reproduce the details of the geology and geometry of the Himalaya–Tibet orogeny; instead, we use them as a conceptual tool to explore how broad rock uplift patterns can affect drainage networks. By incorporating (*i*) a numerical solution to the detachment-limited stream power model for fluvial erosion and (*ii*) an analytical solution for hillslope erosion processes on a dynamic, irregular grid, DAC is designed to efficiently simulate large-scale geomorphic processes (*SI Appendix*). Running DAC on a 400 × 200-km domain over 30 Ma, we first applied a constant rock uplift rate over a large region of the model, allowing the channel network to reach a steady state (Fig. 4 *A* and *B*). We

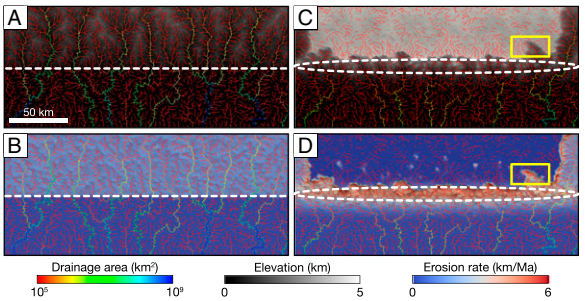

Fig. 4. Conceptual landscape evolution model using the code DAC (51). The model is run over a 400 × 200-km domain for 30 My; two timesteps are shown here (for full model details, see *SI Appendix*). In all panels, the drainage network is colored according to drainage area. In the first time step shown (*A* and *B*), the region north of the white dashed line experiences a constant rock uplift rate of 1.5 km/Ma, whereas the region south experiences a rock uplift rate of 0.3 km/Ma. *A* shows elevation and *B* shows erosion rates at 6 My into the model run, as the channel network approaches a steady-state configuration. Then, at 15 My into the run, a band of faster rock uplift at 2.7 km/Ma is applied within white dashed oval in *C* and *D*. In the second time step shown at 19 My (*C* and *D*), erosion rates behind the band of high rock uplift rates decrease significantly (*D*), but because the rock uplift rate in this region is still positive surface uplift occurs and a broad low-relief, high-elevation plateau develops (*C*). Within this plateau, we observe features similar to those observed in southeastern Tibet, including isolated lakes and unusual channel geometries. We also observe a river that begins to incise the plateau behind the band of high rock uplift rate, highlighted by the yellow box in *C* and *D*, which may be analogous to the Yarlung River.

then applied a higher rock uplift rate in a focused band, as a simplified model of rapid rock uplift caused by duplexing in the Himalaya, to predict how the channel network would respond (Fig. 4 *C* and *D*). Rock uplift rates outpace river incision along this band, producing several features observed in southeastern Tibet, including (*i*) channel network defeat and consequent river diversion, (*ii*) high-elevation lake formation, and (*iii*) very slow erosion rates in the region immediately north of the band of focused rock uplift (Fig. 4*D*). As a consequence of the very slow erosion rates and continued rock uplift, a high-elevation, low-relief plateau forms in this region that is eventually incised by rivers along its sides (Fig. 4*C*).

In concert with our thermochronometric observations, these simulations indicate that river diversion and consequent reduction of stream power and shutdown of erosion provides a plausible mechanism for sustaining, if not generating, the high elevations and relatively low relief topography of the externally drained southern Tibetan plateau. These results suggests that the southern margin of the Tibetan plateau has persisted not through an increase in rock uplift rate directly, but through a decrease in erosion rate. Further, plateau development in response to decreased erosion rates (Fig. 4) likely plays an important role in plateau generation in convergent orogens more generally, as previously suggested from mechanical numerical models (52, 53).

Ways Forward

Numerous areas of future research can test our ideas about landscape evolution across the southern Tibetan plateau. Although there is significant evidence for drainage reorganization within the southern Tibetan plateau, detailed geologic investigations of the geomorphology and fluvial deposits in intermontane basins north of the present day drainage divide can provide more concrete tests for whether transverse rivers existed before ∼10 Ma. Additionally, if transverse rivers dissected the southeastern Lhasa terrane before ∼10 Ma, there ought to be material derived from the Cenozoic Linzizong Group volcanics (the extrusive counterpart to the Gangdese batholith) and Paleozoic to Mesozoic marine strata from

the Lhasa terrane in Siwalik Group foreland basin deposits of that age, particularly in Bhutan and northeastern India. Last, the timing and severity of aridification and its relative influence on erosion rates in the southern Tibetan plateau is less clear and is not accounted for in our landscape evolution model. The role of precipitation can be explored with coupled climate and tectonomorphic models, as well as geologic studies of Miocene age sediments, to see whether independent evidence exists for the timing of aridification of the southern Tibetan plateau.

ACKNOWLEDGMENTS. We thank A. Zuza and R. Reith for collecting samples, N. Fylstra for laboratory assistance, and Z. Zhao, M. Xuanxue, D. Zhu, F. Meng, and Y. Chen for help with field logistics. This manuscript benefited from stimulating discussions with W. Dietrich, D. DePaolo, and J. Dai and critical reviews from B. Bookhagen and A. Duvall. This work was supported by National Science Foundation (NSF) Continental Dynamics program Grant EAR-1111853 (to. D.L.S., T.M.H., and P.K.Z.), an NSF Graduate Research Fellowship (to M.M.T.), the University of California-Berkeley Larsen grant (to D.L.S.), and the Ann and Gordon Getty Foundation (D.L.S.). The ion microprobe facility at University of California, Los Angeles is partly supported by the NSF Instrumentation & Facilities program (EAR-1339051; to T.M.H.).

1. Hatzfeld D, Molnar P (2010) Comparisons of the kinematics and deep structures of the Zargos and Himalaya and of the Iranian and Tibetan plateaus and geodynamic implications. *Rev Geophys* 48(2):1–48.
2. Rowley DB, Currie BS (2006) Palaeo-altimetry of the late Eocene to Miocene Lunpola basin, central Tibet. *Nature* 439(7077):677–681.
3. DeCelles PG, et al. (2007) High and dry in central Tibet during the Late Oligocene. *Earth Planet Sci Lett* 253(3-4):389–401.
4. Hetzel R, et al. (2011) Peneplain formation in southern Tibet predates the India-Asia collision and plateau uplift. *Geology* 39(10):983–986.
5. Rohrmann A, et al. (2012) Thermochronologic evidence for plateau formation in central Tibet by 45 Ma. *Geology* 40(2):187–190.
6. Haider VL, et al. (2013) Cretaceous to Cenozoic evolution of the northern Lhasa Terrane and the Early Paleogene development of peneplains at Nam Co, Tibetan Plateau. *J Asian Earth Sci* 70-71:79–98.
7. Duvall AR, Clark MK, Avdeev B, Farley KA, Chen Z (2012) Widespread late Cenozoic increase in erosion rates across the interior of eastern Tibet constrained by detrital low-temperature thermochronometry. *Tectonics* 31(3):TC3014.
8. Tian Y, Kohn BP, Hu S, Gleadow AJW (2015) Synchronous fluvial response to surface uplift in the eastern Tibetan Plateau: Implications for crustal dynamics. *Geophys Res Lett* 42(1):29–35.
9. Zheng D, Clark MK, Zhang P, Zheng W, Farley KA (2010) Erosion, fault initiation and topographic growth of the North Qilian Shan (northern Tibetan Plateau). *Geosphere* 6(6):937–941.
10. Spicer RA, et al. (2003) Constant elevation of southern Tibet over the past 15 million years. *Nature* 421(6923):622–624.
11. Currie BS, Rowley DB, Tabor NJ (2005) Middle Miocene paleoaltimetry of southern Tibet: Implications for the role of mantle thickening and delamination in the Himalayan orogen. *Geology* 33(3):181–184.
12. Ding L, et al. (2014) The Andean-type Gangdese Mountains: Paleoelevation record from the Paleocene–Eocene Linzhou Basin. *Earth Planet Sci Lett* 392: 250–264.
13. Lang KA, Huntington KW (2014) Antecedence of the Yarlung–Siang–Brahmaputra River, eastern Himalaya. *Earth Planet Sci Lett* 397:145–158.
14. Bracciali L, Najman Y, Parrish RR, Akhter SH, Millar I (2015) The Brahmaputra tale of tectonics and erosion: Early Miocene river capture in the Eastern Himalaya. *Earth Planet Sci Lett* 415:25–37.
15. Robinson RAJ, et al. (2014) Large rivers and orogens: The evolution of the Yarlung Tsangpo–Irrawaddy system and the eastern Himalayan syntaxis. *Gondwana Res* 26(1): 112–121.
16. Lal D, et al. (2004) Erosion history of the Tibetan Plateau since the last interglacial: Constraints from the first studies of cosmogenic ^{10}Be from Tibetan bedrock. *Earth Planet Sci Lett* 217(1-2):33–42.
17. Dietsch C, Dortch JM, Reynhout SA, Owen LA, Caffee MW (2015) Very slow erosion rates and landscape preservation across the southwestern slope of the Ladakh Range, India. *Earth Surf Process Landf* 40(3):389–402.
18. Shuster DL, Farley KA (2004) 4He/3He thermochronometry. *Earth Planet Sci Lett* 217(1-2):1–17.
19. Lovera OM, Richter FM, Harrison TM (1989) The ^{40}Ar/^{39}Ar thermochronometry for slowly cooled samples having a distribution of diffusion domain sizes. *J Geophys Res* 94(B12):17917–17935.
20. Braun J (2003) Pecube: A new finite-element code to solve the 3D heat transport equation including the effects of a time-varying, finite amplitude surface topography. *Comput Geosci* 29(6):787–794.
21. Zeitler PK, et al. (2014) Tectonics and topographic evolution of Namche Barwa and the easternmost Lhasa block, Tibet. *Toward an Improved Understanding of Uplift Mechanisms and the Elevation History of the Tibetan Plateau*, eds Nie J, Horton BK, Hoke GD, *Geol Soc Am Spec Pap* 507:23–58.
22. Clark MK, et al. (2005) Late Cenozoic uplift of southeastern Tibet. *Geology* 33(6): 525.
23. Copeland P, et al. (1995) Thermal evolution of the Gangdese batholith, southern Tibet: A history of episodic unroofing. *Tectonics* 14(2):223–236.
24. Dai J, Wang C, Hourigan J, Li Z, Zhuang G (2013) Exhumation history of the Gangdese Batholith, Southern Tibetan Plateau: Evidence from apatite and zircon (U-Th)/He thermochronology. *J Geol* 121(2):155–172.
25. Carrapa B, et al. (2014) Miocene burial and exhumation of the India-Asia collision zone in southern Tibet: Response to slab dynamics and erosion. *Geology* 42(5): 443–446.
26. Aikman AB, Harrison TM, Hermann J (2012) Age and thermal history of Eo- and Neohimalayan granitoids, eastern Himalaya. *J Asian Earth Sci* 51:85–97.
27. Li G, et al. (2015) Cenozoic low temperature cooling history of the Northern Tethyan Himalaya in Zedang, SE Tibet and its implications. *Tectonophysics* 643:80–93.
28. Thiede RC, Ehlers TA (2013) Large spatial and temporal variations in Himalayan denudation. *Earth Planet Sci Lett* 371-372:278–293.
29. Harrison TM, Copeland P, Kidd WSF, Lovera OM (1995) Activation of the Nyainqentanghla Shear Zone: Implications for uplift of the southern Tibetan Plateau. *Tectonics* 14(3):658–676.
30. Styron RH, et al. (2013) Miocene initiation and acceleration of extension in the South Lunggar rift, western Tibet: Evolution of an active detachment system from structural mapping and (U-Th)/He thermochronology. *Tectonics* 32(4):880–907.
31. DeCelles PG, Kapp P, Quade J, Gehrels GE (2011) Oligocene-Miocene Kailas basin, southwestern Tibet: Record of postcollisional upper-plate extension in the Indus-Yarlung suture zone. *Geol Soc Am Bull* 123(7-8):1337–1362.
32. Harrison TM, et al. (2000) The Zedong Window: A record of superposed tertiary convergence in southeastern Tibet. *J Geophys Res* 105(B8):19211–19230.
33. Yin A, et al. (1994) Tertiary structural evolution of the Gangdese Thrust System, southeastern Tibet. *J Geophys Res* 99(B9):18175.
34. Finlayson DP, Montgomery DR, Hallet B (2002) Spatial coincidence of rapid inferred erosion with young metamorphic massifs in the Himalayas. *Geology* 30(3):219–222.
35. Anders AM, Roe GH, Montgomery DR, Finnegan NJ (2006) Spatial patterns of precipitation and topography in the Himalaya. *Geol Soc Am Spec Pap 398* 2398(03): 39–53.
36. Bookhagen B, Burbank DW (2010) Toward a complete Himalayan hydrological budget: Spatiotemporal distribution of snowmelt and rainfall and their impact on river discharge. *J Geophys Res* 115(F3):F03019.
37. Roe GH (2005) Orographic precipitation. *Annu Rev Earth Planet Sci* 33(1):645–671.
38. Herzschuh U (2006) Palaeo-moisture evolution in monsoonal Central Asia during the last 50,000 years. *Quat Sci Rev* 25(1-2):163–178.
39. Portenga EW, Bierman PR (2011) Understanding Earth's eroding surface with ^{10}Be. *GSA Today* 21(8):4–10.
40. Kohn MJ, Wieland MS, Parkinson CD, Upreti BN (2004) Miocene faulting at plate tectonic velocity in the Himalaya of central Nepal. *Earth Planet Sci Lett* 228(3-4): 299–310.
41. Herman F, et al. (2010) Exhumation, crustal deformation, and thermal structure of the Nepal Himalaya derived from the inversion of thermochronological and thermobarometric data and modeling of the topography. *J Geophys Res* 115(B6): B06407.
42. Tobgay T, McQuarrie N, Long S, Kohn MJ, Corrie SL (2012) The age and rate of displacement along the Main Central Thrust in the western Bhutan Himalaya. *Earth Planet Sci Lett* 319-320:146–158.
43. Coutand I, et al. (2014) Geometry and kinematics of the Main Himalayan Thrust and Neogene crustal exhumation in the Bhutanese Himalaya derived from inversion of multithermochronologic data. *J Geophys Res Solid Earth* 119(2):1446–1481.
44. Hodges KV (2000) Tectonics of the Himalaya and Southern Tibet from two perspectives. *Bull Geol Soc Am* 112(3):324–350.
45. Yin A (2006) Cenozoic tectonic evolution of the Himalayan orogen as constrained by along-strike variation of structural geometry, exhumation history, and foreland sedimentation. *Earth Sci Rev* 76(1-2):1–131.
46. Cina SE, et al. (2009) Gangdese arc detritus within the eastern Himalayan Neogene foreland basin: Implications for the Neogene evolution of the Yalu–Brahmaputra River system. *Earth Planet Sci Lett* 285(1-2):150–162.
47. Bollinger L, et al. (2004) Thermal structure and exhumation history of the Lesser Himalaya in central Nepal. *Tectonics* 23(5):TC5015.
48. Koons PO, Zeitler PK, Hallet B (2013) Tectonic aneurysms and mountain building. *Treatise on Geomorphology*, eds Schroder J, Owen LA (Academic Press, San Diego), pp 318–349.
49. Zeitler PK, et al. (2001) Erosion, Himalayan geodynamics, and the geomorphology of metamorphism. *GSA Today* 11(1):4–8.
50. Wang P, et al. (2014) Tectonic control of Yarlung Tsangpo Gorge revealed by a buried canyon in Southern Tibet. *Science* 346(6212):978–981.
51. Goren L, Willett SD, Herman F, Braun J (2014) Coupled numerical-analytical approach to landscape evolution modeling. *Earth Surf Process Landf* 39(4):522–545.
52. Willett SD (1999) Orogeny and orography: The effects of erosion on the structure of mountain belts. *J Geophys Res* 104(B12):28957.
53. Beaumont C, Jamieson RA, Nguyen MH, Lee B (2001) Himalayan tectonics explained by extrusion of a low-viscosity crustal channel coupled to focused surface denudation. *Nature* 414(6865):738–742.